Post-print of: Lachowicz J., Rucka M.: 3-D finite-difference time-domain modelling of ground penetrating radar for identification of rebars in complex reinforced concrete structures. Archives of Civil and Mechanical Engineering. Vol. 18, iss. 4 (2018), p. 1228-1240. DOI: 10.1016/j.acme.2018.01.010

3-D finite-difference time-domain modelling of ground penetrating radar for identification of rebars in complex reinforced concrete structures

Jacek Lachowicz*, Magdalena Rucka

Department of Mechanics of Materials and Structures
Faculty of Civil and Environmental Engineering
Gdańsk University of Technology
ul. Narutowicza 11/12, 80-233 Gdańsk, Poland
emails: jacek.lachowicz@pg.edu.pl, magdalena.rucka@pg.edu.pl

Abstract

This paper presents numerical and experimental investigations to identify reinforcing bars using the ground penetrating radar (GPR) method. A novel element of the paper is the inspection of different arrangements of reinforcement bars. Two particular problems, i.e. detection of few adjacent transverse bars and detection of a longitudinal bar located over or under transverse reinforcement, have been raised. An attention was also paid to the influence of few adjacent bars on the estimation of wave velocity in concrete based on the diffraction hyperbola. The GPR simulations were undertaken using the finite-difference time-domain (FDTD) method. The new approach for the numerical modelling of GPR in complex reinforced concrete structures with the use of a 3-D FDTD model was presented. Simulated scans for the 3-D model were compared with results of in-situ surveys. The results of investigations showed high usefulness of the 3-D model for the GPR field propagation in structures with a complex system of the reinforcement.

Keywords

ground penetrating radar; 3-D finite-difference time-domain modelling; reinforced concrete structures; reinforcing bars; hyperbola fitting

1. Introduction

Recently, there has been a growing interest in developing non-destructive testing techniques for the assessment of civil engineering objects [1]. Considering structures made of reinforced concrete, the important issue is the inspection of reinforcing bars. Some methods have proven to be particularly useful in the examination of steel rebars, like the use of a magnetic field imaging camera to estimate the depth and diameter of reinforcement [2] or the use of X-rays to estimate the reinforcement position [3]. However, the most common approach in the inspection of reinforced concrete structures is the application of the ground penetrating radar (GPR). This method has found many applications in the evaluation of bridges [4], [5], tunnels [6], road pavements [7], retaining walls [8] or buildings [9]. The previous studies indicated a large potential of the GPR method in the identification of the amount, position, distribution [10] and diameter of rebars in concrete specimens [11] with a simple arrangement of reinforcement. Conducted research also involved the influence of the bar spacing on the GPR maps [12] or the possibility of detection of various type defects near the reinforcing bars [13]. However, considering structures with a complicated reinforcement system, difficulties connected with the interpretation of GPR maps may arise. In such cases, numerical modelling of propagation of electromagnetic field using finite-difference time-domain (FDTD) method becomes a powerful tool that enables understanding the origin of reflections appearing in GPR radargrams. A wide range of studies has already been reported on the GPR simulations with the use of 2-D FDTD models. Numerical calculations were used as a tool for interpretation of measurement results for reinforced concrete [6], masonry [14] and stone [15,16] structures. In addition, 2-D modelling allowed to verify invented processing algorithms of GPR data [17]. At present, researchers are starting to implement 3-D FDTD models for GPR simulations, but still current applications of 3-D analyses are mainly concentrated on complex modelling of soil [18], [19] and bricks [20].

This study presents numerical and experimental investigations to identify reinforcing bars using the GPR method. In previous studies [21,22] initial research concerning the possibilities of the use of 2-D and 3-D numerical modelling in the interpretation of GPR maps were conducted. A novel element of the paper is the inspection of different arrangements of reinforcement bars. Typically, GPR investigations concern single bars distributed at the regular spacing for which multiple hyperbolas are obtained in radargrams. In this study, the problem of detection of few adjacent bars is considered resulting in the deformation of the hyperbolic curve. A particular attention is paid to the influence of the adjacent bars on the estimation of

wave velocity in concrete. Another issue raised in the study is the detection of a longitudinal bar located over or under the transverse reinforcement. The paper also presents the new approach for the numerical modelling of GPR in reinforced concrete structures with a complex system of the reinforcement with the use of a 3-D FDTD model on the example of a frame arch pedestrian bridge. Simulated scans for the 3-D model were compared with results of in-situ surveys.

2. The object and problem description

The object of investigations was a reinforced concrete pedestrian bridge (Fig. 1a, b). The bridge is a frame arch structure with a theoretical span of 28 m. The bridge deck with a thickness of 50 cm is supported on the abutments and on the key of the arch. On both sides of the main part of the deck, cantilever slabs of varying thickness between 20 cm and 25 cm were designed. The tested structure was chosen because of the complex reinforcement system. Figure 1c presents the reinforcement drawing based on the technical documentation. The main longitudinal reinforcement of the structure consists of bars of 12 mm diameter with a spacing of 10 cm. The lower reinforcement of the deck includes bars of 32 mm diameter with a spacing of 10 cm. The transverse reinforcement with a diameter of 12 mm consists of three rows of rebars: two rows of stirrups in the deck and one curved rod in the cantilever part. The structure was made of concrete C30/37.

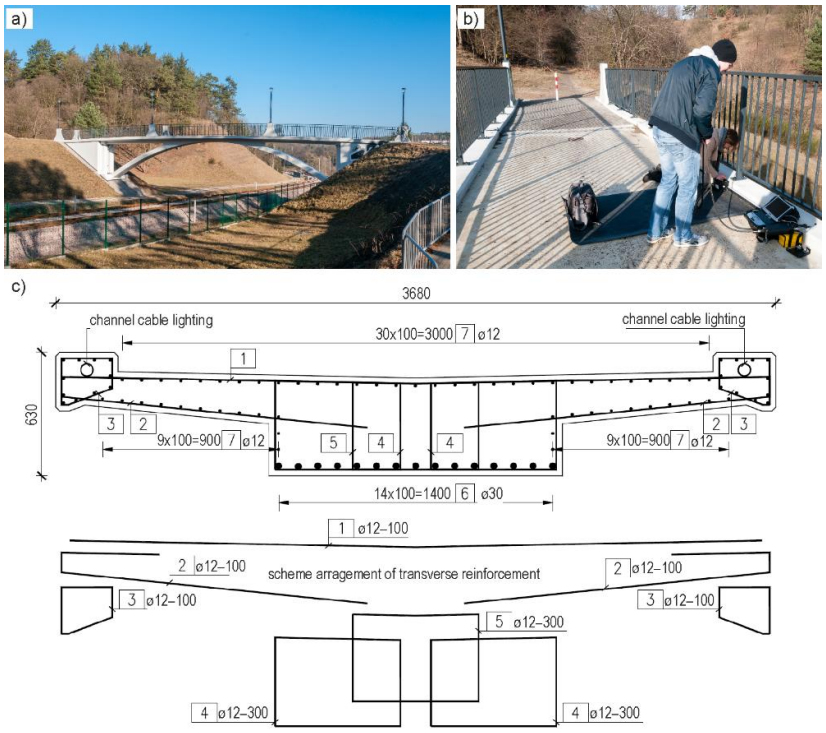

Fig. 1. Considered reinforced concrete pedestrian bridge (Gdańsk, Poland, 54°21'32.4"N 18°34'01.8"E): (a) general view; (b) deck during GPR measurements; (c) cross-section of the bridge with reinforcement drawing (dimensions in mm)

The presented reinforcement system reveals several problems that may arise in the interpretation of GPR data. The first issue concerns the number of bars that are located close to each other. Figure 2a shows a concrete section with a single embedded bar. In such a case, the diffraction by the circular inclusion is represented as a hyperbola. When few adjacent bars are embedded in concrete, the hyperbolic curve is deformed and the signal becomes stronger (Fig. 2b). Another problem is the mutual arrangement of longitudinal and transverse rebars. If the transverse bar is situated over the longitudinal bar, the hyperbola is cut off at the level of the longitudinal bar (Fig. 2c). If the transverse bar is situated under the longitudinal bar, the hyperbola appears under the longitudinal reflection without major changes (Fig. 2d).

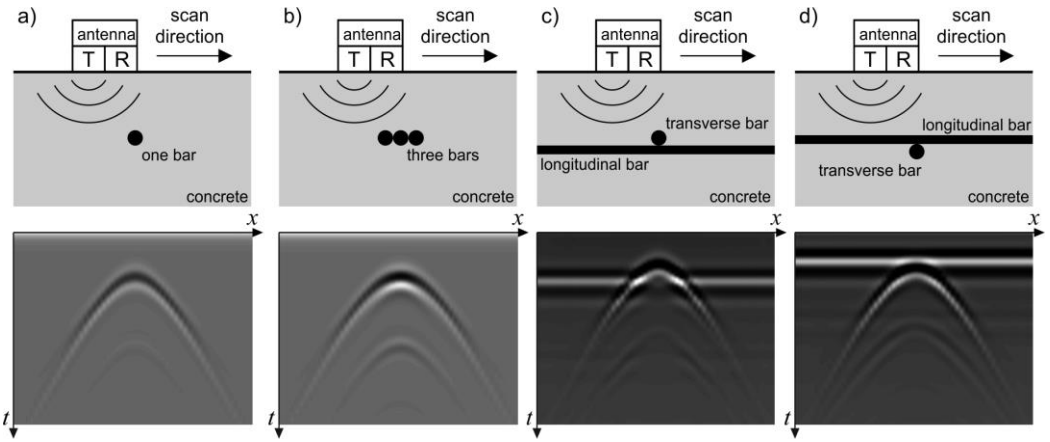

Fig. 2. Different situations of bar location: (a) single bar; (b) three adjacent bars in a row; (c) transverse bar over longitudinal bar; (d) longitudinal bar over transverse bar

3. Materials and methods

3.1. Mathematical models of diffraction hyperbola

The electromagnetic wave diffracted from a circular inclusion having different electrical properties reveals on a GPR map as a hyperbolic curve. The simplest mathematical model of the diffraction hyperbola is presented in Fig. 3a and described by the following relation [23]:

$$t = \sqrt{\frac{4\left(x_i - x_0\right)^2}{v^2} + t_0^2} \tag{1}$$

where x_0 is the location of the inclusion, t_0 is the two-way travel time to the inclusion, x_i is the radar position and v denotes the velocity of electromagnetic waves in the considered medium. The approach reduces the inclusion to a point and neglects the distance between the transmitting and receiving antenna. The extension of Eq. (1) to the case taking into account the actual bar radius R and the distance s between the transmitting and receiving antennas (Fig. 3b) gives (e.g. [24]):

$$t = \frac{1}{v}\left(\sqrt{\left(\frac{vt_0}{2}+R\right)^2+\left(x_0-x_i-\frac{s}{2}\right)^2}+\sqrt{\left(\frac{vt_0}{2}+R\right)^2+\left(x_0-x_i+\frac{s}{2}\right)^2}-2R\right) \quad (2)$$

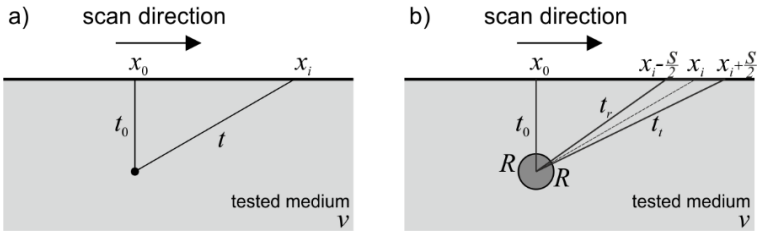

Fig. 3. Geometrical relationship for derivation of diffraction hyperbola caused by circular inclusion: (a) with zero radius; (b) with radius *R* and the distance *s* between the transmitting and receiving antennas

The identification of hyperbolas on a GPR map enables the estimation of the velocity of propagated waves and then a determination of the relative permittivity ε_r of a medium in which the bar is embedded. The fitting of the hyperbola described by Eq. (1) into a GPR map can be performed by the direct least square method, while in the case of the hyperbola described by Eq. (2) a nonlinear method of approximation has to be used (e.g. Levenberg-Marquardt method [25]).

3.2 FTDT simulations

Numerical analyses of electromagnetic wave propagation were carried out using the open-source gprMax (version: 3.0.19) software [26,27] based on the finite-difference time-domain method [28]. This method solves Maxwell's equations with the appropriate boundary and initial conditions using the central finite differences. The calculations were performed using both 2-D and 3-D models. The advantage of 2-D models is a relatively short time of calculations, so it is possible to use small Yee cells. However, the geometry is considered to be infinite in the third direction, so it is necessary to create a separate model for each scan trace, if the object has variable geometry along its length. Therefore 2-D models are suitable for calculations of concrete structures with simple reinforcement, without rebars parallel to a scan trace. The advantage of 3-D models is the fact that just one geometry is built and scan routes can be arbitrarily selected. Such 3-D models are suitable for analysing structures with a complex reinforcement system. However, to decrease the time of calculations, larger Yee cells are required which may cause a worse representation of small rebars and be a reason for numerical dispersion.

In order to demonstrate selected problems of rebars identification, GPR simulations in two structures, i.e. a concrete slab and the considered bridge, were conducted. The material parameters have been adopted in accordance with the results of in-situ surveys. The value of

the electric permittivity of concrete was determined as ε_r = 6.25 and the conductivity of concrete was adopted as σ = 0.01 S/m. A source excitation imitating a signal generated by the GPR antenna was applied as the Ricker function with a frequency of 2 GHz. The time step was selected automatically based on the CFL condition depending on the size of the Yee cell. At the edges of the FDTD model, the perfectly match layer (PML) absorbing boundary conditions were set up. The distance between the transmitting and receiving antenna in the model was set to 6 cm like the actual distance between the transmitter and receiver in the IDS antenna.

A 2-D model of the concrete slab (Fig. 4) with dimensions of 195 cm × 30 cm was considered to verify the theoretical assumptions for estimation of the velocity of electromagnetic waves based on the diffracted hyperbola. Simulated area of concrete with a thickness of 20 cm contains embedded steel bars with a spacing of 45 cm. In the first case (model no. 1 shown in Fig. 4a), the slab contains four bars with different radius (R = 6 mm, 12 mm, 18 mm and 24 mm). In the second case (model no. 2 shown in Fig. 4b), the same slab was considered for varying number of adjacent bars of the same diameter, but different number. This case reproduces stirrups in reinforced concrete structures, which are often placed next to each other (see Fig. 1c and Fig. 2b).

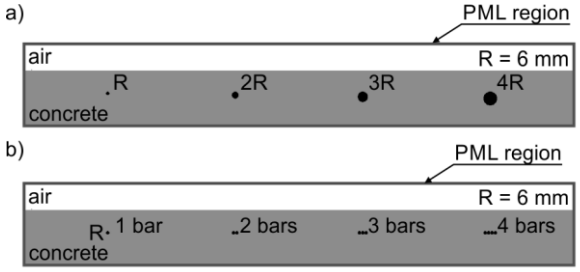

Fig. 4. Concrete slab reinforced by steel bars: (a) model no.1 (four single bars with different radius); (b) model no. 2 (single bar, 2, 3 and 4 adjacent bars with the same radius)

The 3-D numerical model of the reinforced concrete pedestrian bridge was created with a particular attention on the distribution of the transverse reinforcement (cf. Fig. 1). All the rebars from the project were included in the model. There has been only a simplification of the inclination of the pavement. It was assumed that the pavement is straight. Furthermore, a layer of the pavement was not included in the model. The 3-D model is shown in Fig. 5. The outer dimensions of the model were: 368 cm × 65 cm × 60 cm. The cubic Yee cells with a size of 3 mm were applied. FDTD simulations for the transverse scan lasted 99 hours (PC, 4 core 8 threads CPU @ 3.40 GHz, 16 GB of RAM). Calculations were carried out for two transverse (along the bridge width) and six longitudinal (along the bridge length) scans. The transverse scans were assumed exactly over and between the transverse reinforcement. In

order to show reflections and to examine the possibility of detection of several rows of the transverse reinforcement, longitudinal scans were calculated in six cross-sections of the bridge marked in Fig. 5b. Sections A-A, B-B and C-C show the cases of transverse bars connected together for one, two or three rebars respectively. Sections D-D, E-E and F-F show the case when the scan is acquired directly over the longitudinal reinforcement for one, two and three adjacent stirrups.

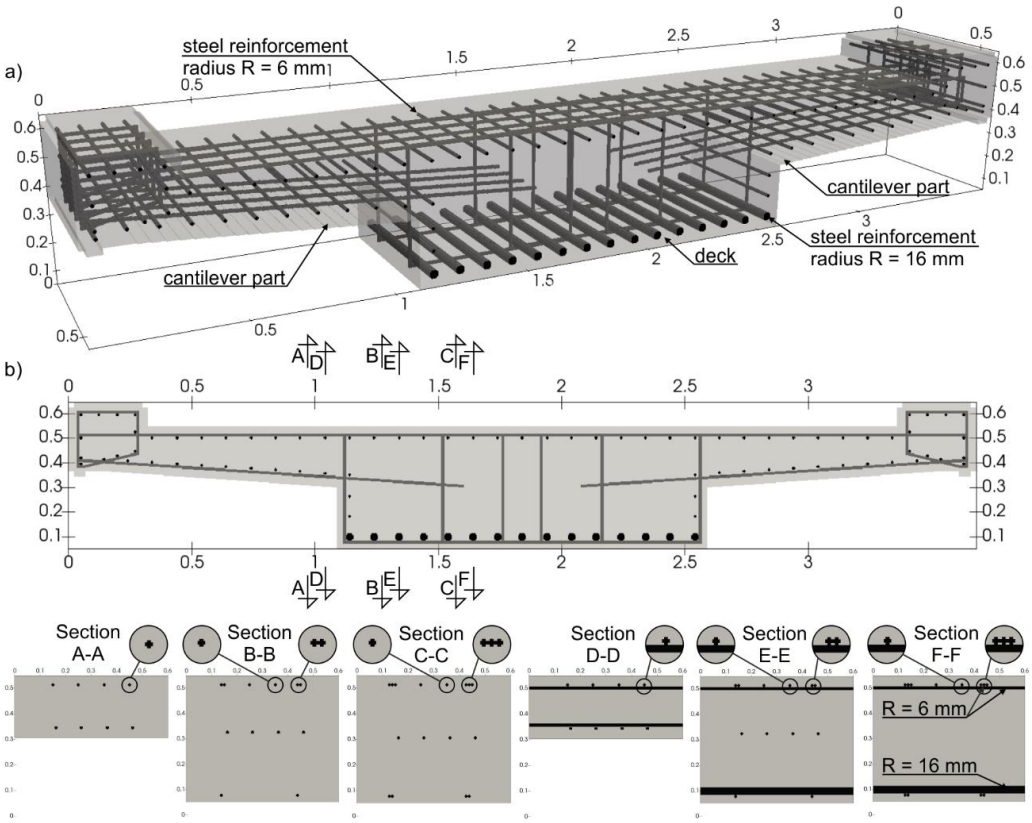

Fig. 5. Numerical 3-D model of the considered bridge: (a) the system of the reinforcement; (b) 2-D view with marked sections A-A, B-B, C-C, D-D, E-E, F-F

3.3. GPR surveys

In-situ measurements of the considered bridge (Fig. 1) were performed using Aladdin system from IDS GeoRadar. A bipolar antenna operating with a central frequency of 2 GHz provided high-resolution echogram, however, reducing the effective penetration depth up to about 0.5 m. The survey parameters were: 32 ns range, 1024 samples per scan, 1 cm step. The GPR data were collected using K2 FastWave software (manufacturer: IDS GeoRadar, version: 2.02.000) and processed in GRED HD (manufacturer: IDS GeoRadar, version: 01.06.002) software. GPR surveys were performed to inspect the amount and the distribution of the reinforcement. During the experimental study transverse profiles were performed along the width of the footbridge in different sections with various reinforcement distribution. Along the entire footbridge, longitudinal scans were carried out on the cantilever part and

over the deck. In order to verify precisely the transverse reinforcement of the bridge, a dedicated Pad Survey Guide (PSG) was applied. Figure 1b presents the bridge deck during GPR measurements with the use of PSG mat. The mat containing parallel grooves at a distance of 0.78 cm allowed accurate guidance of 110 transverse traces. Such dense measurements ensured that some of the scans were acquired exactly over the transverse reinforcement.

4. Results and discussion

4.1. Estimation of velocity of electromagnetic waves

The simulations on the models of the concrete slab (Fig. 4) were intended to assess the possibility of the estimation of the wave propagation velocity for the unknown number of adjacent bars. The data were processed in the MATLAB® environment (manufacturer: The MathWorks, Inc., version: 9.1.0.441655). From the simulated B-scans, individual points were extracted selecting the minimum value of the voltage for each A-scan. Next, the approximation process was applied using Eqs. (1) and (2). Numerical GPR maps with marked extracted points and fitted hyperbolas for models no. 1 and no. 2 are illustrated in Fig. 6a and Fig. 6b, respectively. Depending on the number of bars and the radius value, the strength of the diffraction changes. Figures 6c and 6d show the voltage for A-scans over particular bars. In model no. 1 containing one bar with various diameter, the increase of the voltage with the increase of bar diameter is observed but not significant (Fig. 6c). In contrast, in model no. 2 containing the different number of adjacent bars, the significant increase of the amplitude with the increasing number of bars can be observed (Fig. 6d).

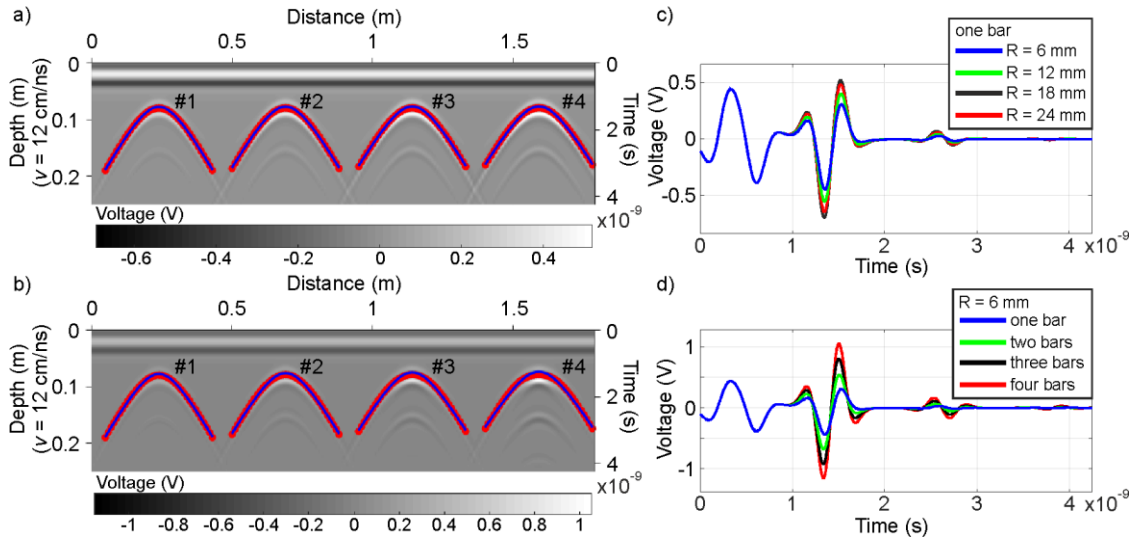

Fig. 6. Simulated GPR maps for a concrete slab reinforced by steel bars with extracted points and approximated hyperbolas: (a) model no. 1 (four single bars with different radius); (b) model no. 2 (single bar, 2, 3 and 4 adjacent bars with the same radius); and simulated A-scans over bars: (c) model no. 1; (d) model no. 2

The results of the estimation of the velocity of the electromagnetic wave propagation are presented in Table 1. In model no. 1 the approximation process using Eq. (1) revealed that the identified velocity increases with the increasing bar radius, however, its value is overestimated. Application of Eq. (2) allowed to obtain the velocity value closer to the real one. It is slightly underestimated, but it is almost constant for various values of the radius. The radius is overestimated, but an increasing tendency can be noticed. Even if in the fitting process the velocity or the radius were blocked, it was not possible to estimate the parameters properly. In model no. 2, where the geometrical arrangement of bars does not correspond to the mathematical models described in Section 3.1, the fitting process was performed to check whether it is possible to roughly estimate the velocity or the number of bars using these models. The velocity obtained using Eq. (1) increases with the number of bars and its value is overestimated. The values of the velocity achieved using Eq. (2) are closer to the real ones with the exception of the case of four adjacent bars, because this hyperbola is strongly distorted making it impossible to determine the velocity value correctly. When the velocity value was blocked, it was also not possible to estimate the correct value of the diameter, however, an upward trend can be observed. In both models of the deck, the correlation coefficient r indicating the quality of the hyperbola fitting achieves greater value for approximation based on Eq. (2).

Table 1. Results of hyperbola fitting for the simulated GPR maps (concrete slab reinforced by steel bars)

	hyperbola no			#1	#2	#3	#4
Model 1	Eq. (1)	v	cm/ns	13,16	13,47	13,78	14,07
		r	-	0,999706	0,999593	0,999416	0,999363
	Eq. (2)	v	cm/ns	12,11	11,97	11,64	11,58
		R	cm	1,84	2,82	4,25	5,02
		r	-	0,999995	0,999994	0,999995	0,999997
	Eq. (2) blocked velocity	v	cm/ns	12,00	12,00	12,00	12,00
		R	cm	2,27	2,66	3,68	4,24
		r	-	0,999989	0,999993	0,999876	0,999938
	Eq. (2) blocked radius	v	cm/ns	12,72	12,76	12,76	12,81
		R	cm	0,60	1,20	1,80	2,40
		r	-	0,999952	0,999932	0,999864	0,999858
Model 2	Eq. (1)	v	cm/ns	13,16	13,68	14,25	14,88
		r	-	0,999706	0,999233	0,998188	0,996426
	Eq. (2)	v	cm/ns	12,11	11,09	11,89	10,40
		R	cm	1,84	5,33	4,74	10,00
		r	-	0,999995	0,999990	0,999409	0,998773
	Eq. (2) blocked velocity	v	cm/ns	12,00	12,00	12,00	12,00
		R	cm	2,27	3,16	4,50	5,90
		r	-	0,999989	0,999906	0,999369	0,997915

The approximation process was also carried out in order to estimate the average velocities of the electromagnetic waves based on results of in-situ surveys. Considering the fact that the hyperbolas overlap due to the small spacing, an algorithm of extraction of points

was created. Several points along the hyperbola on a GPR map were marked and the interpolation was performed. Then maximum voltage values were extracted at a given distance from the interpolated curve. The fitting of hyperbola was conducted for experimental longitudinal and transverse scans (Fig. 7). Figure 7a presents the experimental transverse radargram without any gain and filters on which the estimation process was performed. The obtained velocities for seven hyperbolas diffracted over bars with the same radius are given in Table 2. The approximation process using Eq. (1) gives slightly higher values of the velocity than using Eq. (2) with the blocked radius. However, when parameters in the curve fitting process may assume any value, the results obtained using Eq. (2) are not satisfying. Measures of variability (standard deviation SD, coefficient of variation CV) of identified wave velocity based on seven hyperbolas from the transverse scan are: SD = 0.147, CV = 0.011 (using Eq.(1)), SD = 1.679, CV = 0.167 (using Eq.(2)) and SD = 0.23, CV = 0.019 (using Eq.(2) with blocked radius).

Table 2. Results of hyperbola fitting for the experimental transverse GPR map

hyperbola no			#1	#2	#3	#4	#5	#6	#7
Eq. (1)	*v*	cm/ns	12,79	13,11	12,91	12,76	13,10	12,97	13,09
	r	-	0,9848	0,9934	0,9931	0,9910	0,9924	0,9955	0,9897
Eq. (2)	*v*	cm/ns	11,83	9,55	7,98	11,42	9,44	8,20	11,92
	R	cm	1,60	6,90	9,54	1,98	6,22	8,76	1,41
	r	-	0,9806	0,9936	0,9910	0,9890	0,9907	0,9950	0,9846
Eq. (2) blocked radius	*v*	cm/ns	12,36	12,79	12,29	12,09	12,58	12,24	12,40
	R	cm	0,60	0,60	0,60	0,60	0,60	0,60	0,60
	r	-	0,9790	0,9908	0,9895	0,9879	0,9885	0,9937	0,9842

Figures 7b and 7c illustrate two experimental longitudinal B-scans. One of the scans was acquired along the bridge over the cantilever part (Fig. 7b) where single bars were supposed to be embedded. The second radargram was acquired along the bridge over the deck (Fig. 7c) where every third stirrup was embedded as two adjacent bars. The results of the fitting are presented in Table 3. Measures of variability (standard deviation SD, coefficient of variation CV) of identified wave velocity based on eight hyperbolas (over a single rod) from longitudinal scans are: SD = 0.263, CV = 0.02 (using Eq.(1)), SD = 1.733, CV = 0.146 (using Eq.(2)) and SD = 0.223, CV = 0.018 (using Eq.(2) with blocked radius). The velocities for the case of two adjacent bars (Fig. 7c) were found to be higher than in case of one single rod (Fig. 7b).

Finally, the average velocity based on experimental diffraction hyperbolas caused by single bars was determined as about 12 cm/ns. The velocity value was validated using a method known as “depth to known reflector method” [29]. Using this method, the velocity was identified as 11,85 cm/ns.

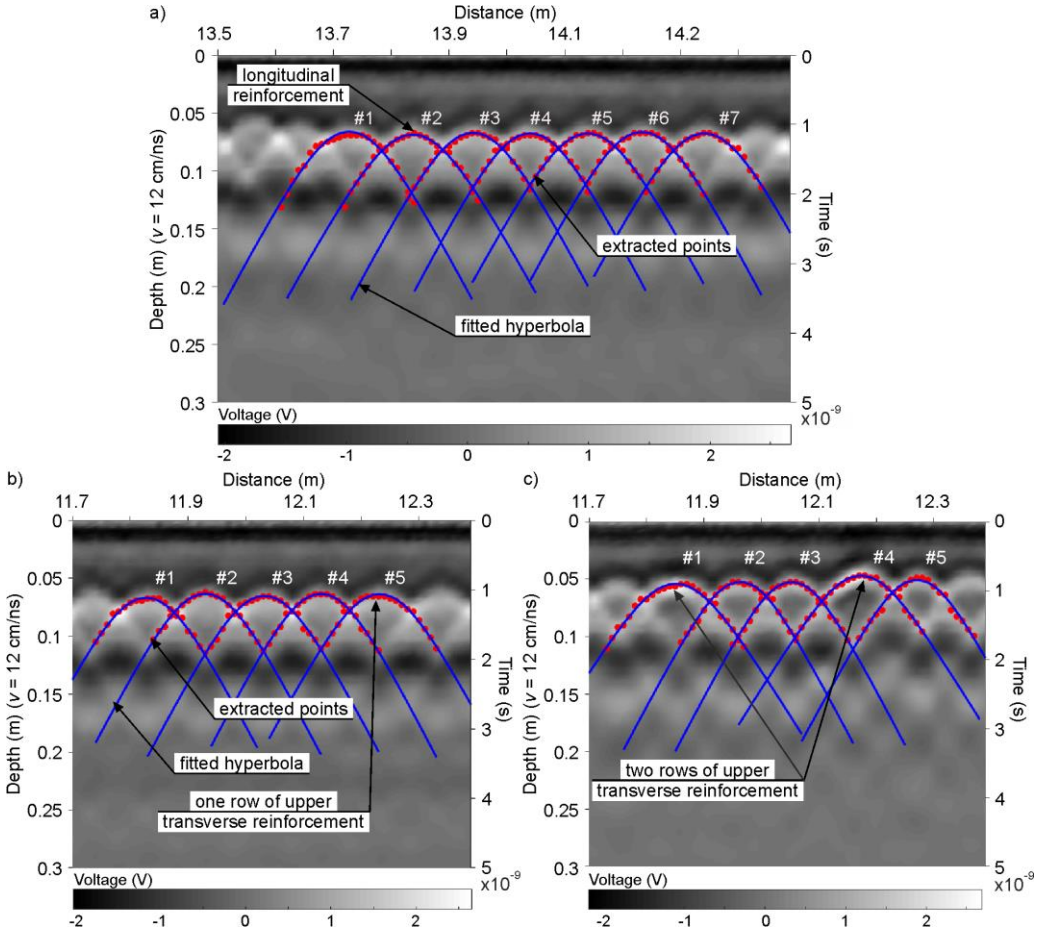

Fig. 7. Experimental GPR maps with extracted points and approximated hyperbolas (a) transverse (b) longitudinal over the cantilever part; (c) longitudinal over the deck

Table 3. Results of hyperbola fitting for the experimental longitudinal GPR maps

	hyperbola no			#1	#2	#3	#4	#5
over the cantilever part	Eq. (1)	*v*	cm/ns	13,08	13,00	12,91	12,78	13,26
		r	-	0,9922	0,9978	0,9932	0,9967	0,9890
	Eq. (2)	*v*	cm/ns	7,61	12,32	12,47	12,18	12,52
		R	cm	10,00	0,30	0,30	0,30	0,76
		r	-	0,9886	0,9945	0,9878	0,9937	0,9841
	Eq. (2) radius blocked	*v*	cm/ns	12,10	12,13	12,17	11,95	12,52
		R	cm	0,60	0,60	0,60	0,60	0,60
		r	-	0,9873	0,9945	0,9878	0,9936	0,9839
over the deck	Eq. (1)	*v*	cm/ns	15,25	13,28	13,12	15,47	13,64
		r	-	0,9924	0,9953	0,9970	0,9966	0,9940
	Eq. (2)	*v*	cm/ns	9,31	12,52	12,43	14,11	12,89
		R	cm	10,00	0,31	0,30	1,14	0,30
		r	-	0,9908	0,9923	0,9945	0,9948	0,9836
	Eq. (2) radius blocked	*v*	cm/ns	14,45	12,30	12,22	14,53	12,62
		R	cm	0,60	0,60	0,60	0,60	0,60
		r	-	0,9887	0,9922	0,9944	0,9948	0,9833

4.2. Inspection of reinforcing bars in the bridge

Figure 8 shows the GPR transverse maps calculated over and between the transverse reinforcement for the 3-D model. In both radargrams, strong and regular hyperbolas are visible giving information about the upper main reinforcement. The lower main reinforcement was possible to detect only in the cantilever part of the bridge. The boundary between the concrete and the air is also noticeable. Particularly noteworthy is the difference between the scan exactly over the transverse reinforcement (Fig 8b) and between the stirrups (Fig 8a). Above the row of hyperbolas on the entire length of the echogram, a longitudinal reflection reveals the presence of the transverse bar. In addition, at places where there is more than one row of transverse bars, a multiple and stronger longitudinal reflection, which slightly deforms the shape of the hyperbolas, can be noticed.

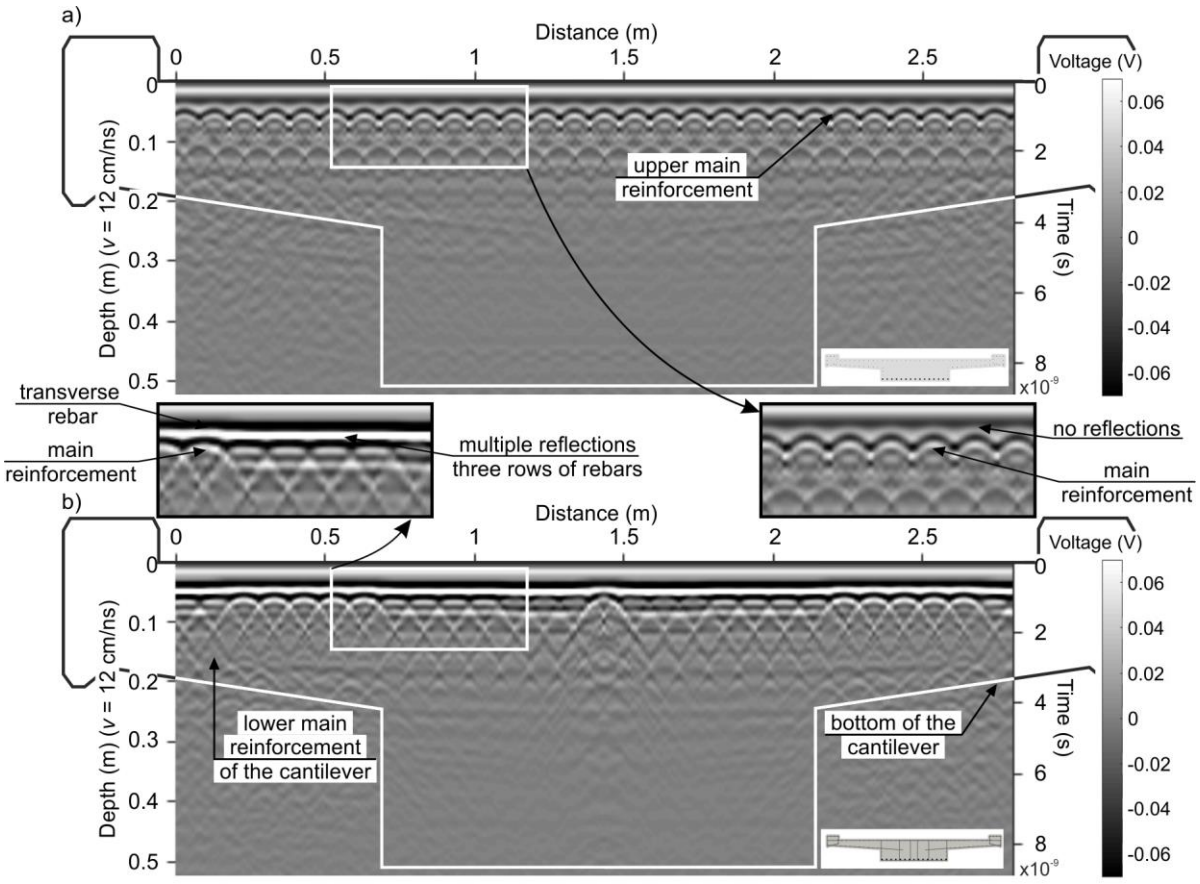

Fig. 8. Simulated transverse GPR maps for 3-D model: (a) scan between transverse reinforcement; (b) scan over transverse reinforcement

Results of in-situ surveys through the bridge cross-section are given in Fig. 9. Figure 9a illustrates a single transverse scan acquired along the width of the bridge. Regular, strong and clear reflections from the upper longitudinal reinforcement can be observed. In addition, a reflection from the bottom of the cantilever part is clearly visible. Above the boundary

between the air and the concrete, hyperbolic diffractions from the lower main reinforcement of the cantilever part of the deck can be noticed. The GPR maps obtained in measurements with the use of the PSG mat are shown in Fig 9b and 9c. The B-scan, which was taken exactly over the transverse reinforcement (Fig. 9a) is clearly different from the scan made between the transverse rebars (Fig. 9b). The transverse reinforcement can be identified as a longitudinal reflection above the hyperbolas.

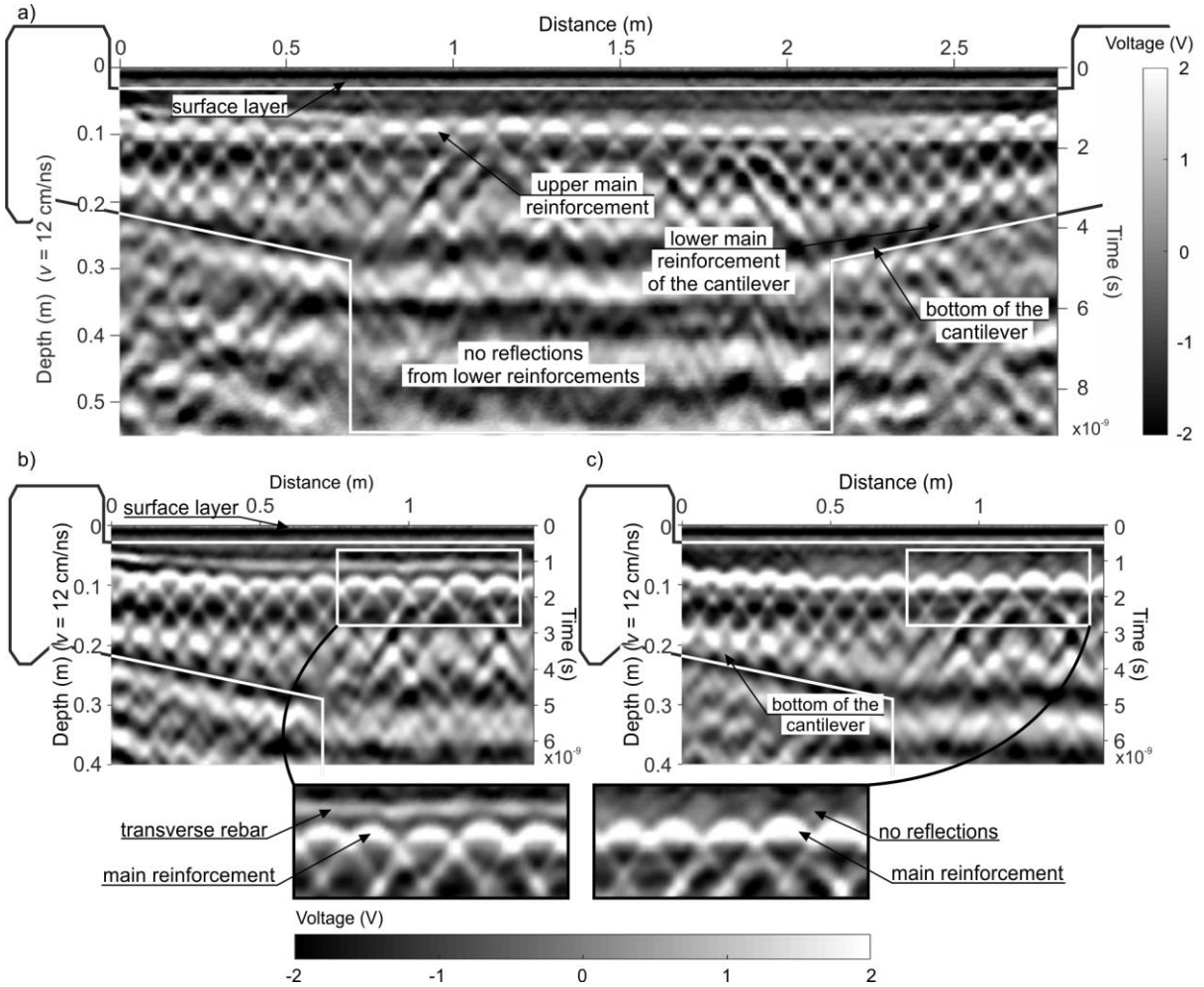

Fig. 9. GPR transverse maps obtained from in-situ surveys using PSG mat: (a) scan over entire cross-section (b) scan over the transverse reinforcement (c) scan between the transverse reinforcement

Figure 10 shows longitudinal GPR maps calculated at the cross-sections marked in Fig. 5b. The B-scan on section A-A over the cantilever part of the deck (Fig. 10a) reveals four hyperbolas resulting from the diffraction of the electromagnetic wave by the upper transverse reinforcement. In sections B-B (Fig. 10b) and C-C (Fig. 10c) where two and three adjacent rebars are embedded, the diffraction is stronger than in the case of one single bar. The amplified amplitude of the voltage is also visible in Fig. 10g where A-scans over the first hyperbola are presented. Results for sections D-D, E-E and F-F containing the longitudinal reinforcement below one, two and three adjacent stirrups are given in Figs. 10d, 10e and 10f,

respectively. Apart from the fact that the amplitude of the reflected signal increases with the number of adjacent bars as in previous cases, additionally the signal strength is slightly greater because of the longitudinal rod under stirrups (Fig. 10h). The longitudinal reflection from the main bar limits the hyperbola which becomes cut off. It should also be noted that with the increase of the number of adjacent bars the longitudinal reflections from the main reinforcement becomes less visible.

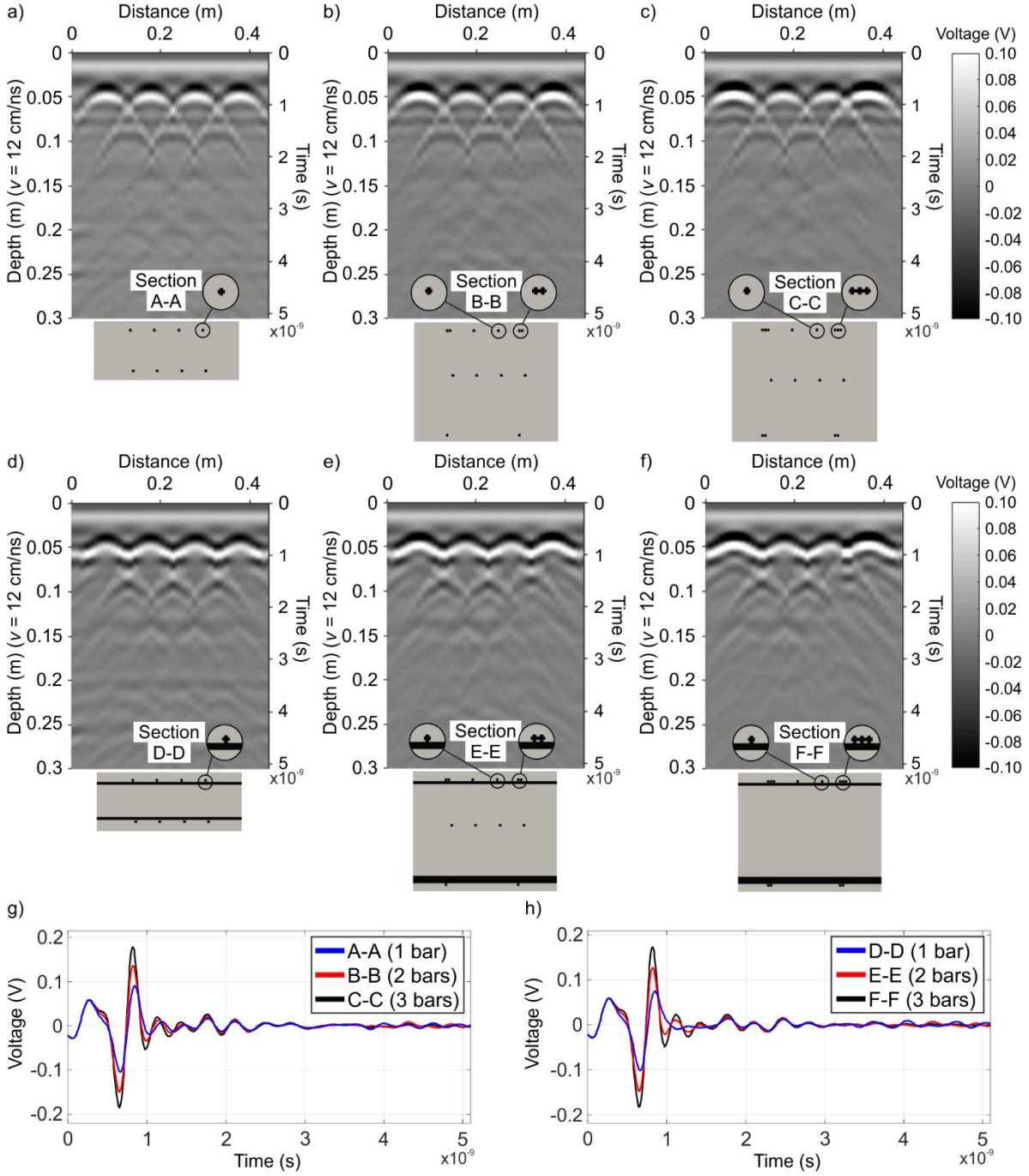

Fig. 10. Simulated longitudinal GPR maps: (a) section A-A; (b) section B-B; (c) section C-C; (d) section D-D; (e) section E-E; (f) section F-F; and simulated A-scans: (g) over the first hyperbola for sections A-A, B-B, C-C; (h) over the first hyperbola for sections D-D, E-E, F-F

The processed longitudinal maps acquired on the main part of the deck and on the cantilever part of the deck are presented in Fig. 11. Two parts of the scanning route were selected, i.e. the distance from 11.7 m to 12.4 m and the distance from 13.6 m to 14.3 m. In the case of the profile over the cantilever part, where there is only one row of the transverse reinforcement, both upper and lower rebars were detected (Fig. 11a). Looking at the echogram acquired over the main part of the deck (Fig. 11b), there is no reflection from the lower bars. The hyperbolas visible in Fig. 11b, between 11.7 m and 12.4 m, come from diffraction of the wave by two adjacent stirrups. Moreover, in the upper layer of bars, multiple hyperbolic diffractions are visible between 13.6 m and 14.3 m. This may be caused by the probable separation between the transverse reinforcement or the appearance of an additional stirrup. It should be emphasized that in the places of occurrence of two reinforcing bars there was a significant increase in the amplitude of reflection as shown in Fig. 11c.

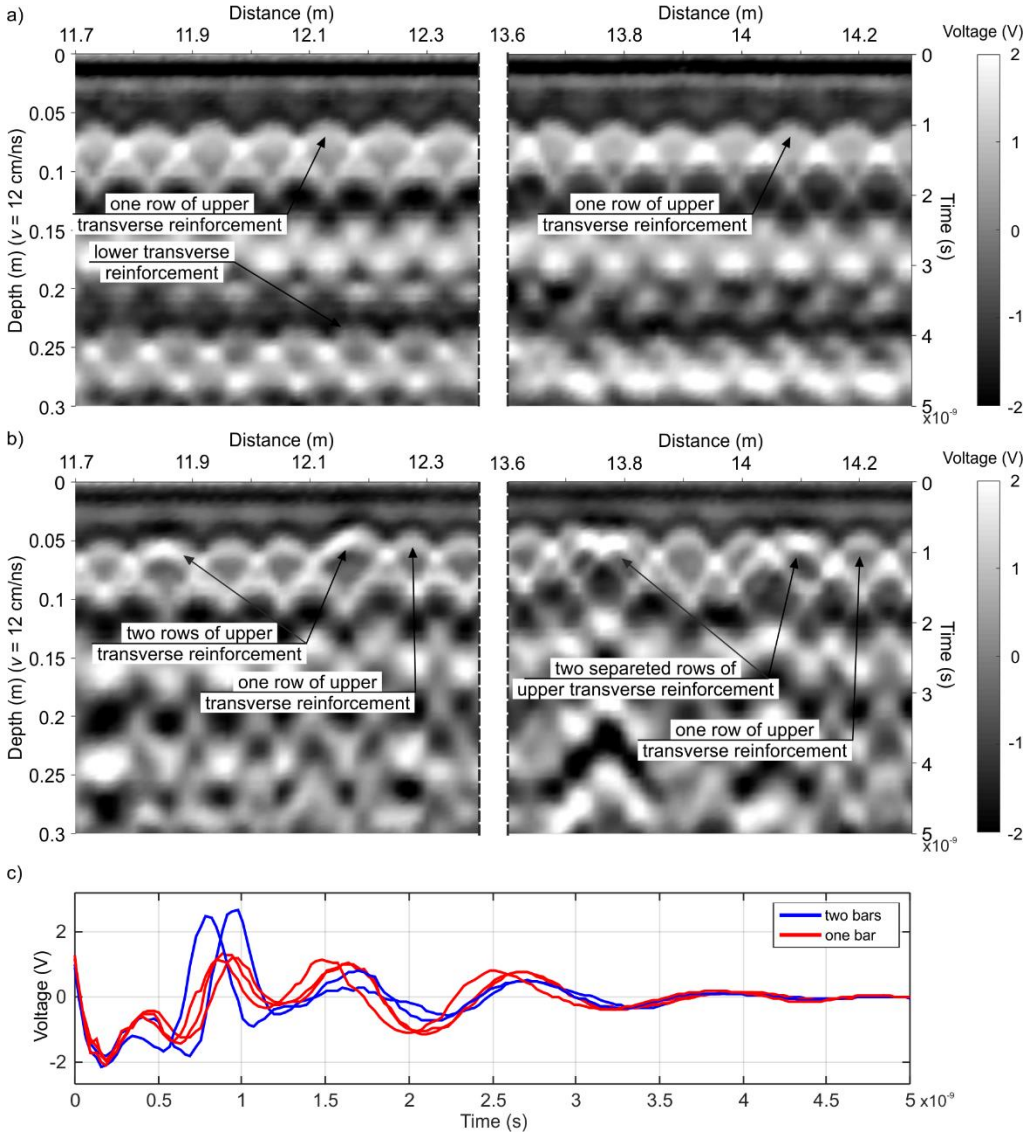

Fig. 11. Experimental longitudinal GPR maps: (a) over the cantilever part; (b) over the bridge deck; and simulated A-scans over bars (c) over the bridge deck

5. Conclusions

In this paper, numerical and experimental studies of electromagnetic wave propagation in concrete structures were carried out by the GPR method. A novel element of the study was the inspection of different arrangements of reinforcement bars in complex concrete structures. Two particular problems, i.e. detection of few adjacent transverse bars and detection of the longitudinal bar located over or under the transverse reinforcement, have been considered. An attention was also paid to the influence of few adjacent bars on the estimation of wave velocity in concrete based on the diffraction hyperbola. Two models of the hyperbola, i.e. the simplest model omitting the bar radius and the model taking into account the radius of the bar and the distance between the transmitting and receiving antennas, were applied for the estimation of the velocity of electromagnetic wave propagation.

The presented numerical and experimental investigations support the following conclusions:

- In the case of the hyperbola fitting based on numerical data, the velocity value determined with the use of the model omitting the radius was overestimated. Moreover, the identified velocity increased with the increasing bar radius or the number of adjacent bars. The use of the model including the bar radius and the separation between antennas allowed to obtain the velocity value closer to the real one and almost constant for various values of the radius. It was found that the velocity can be roughly estimated for the maximum number of three adjacent bars using this model. In the case of four adjacent bars, the hyperbola was strongly distorted making it impossible to determine the velocity value correctly. An improvement in the velocity estimation can be obtained if the radius of the bar is known.
- Considering the hyperbola fitting based on experimental data, the model omitting the bar radius turned out to be less sensitive to measurement noise and hyperbola overlapping than the model including the bar radius with the arbitrary curve fitting parameters. The estimation process based on the model including the bar radius and the separation between antennas was improved, when the radius parameter was established as the radius that was used in the considered structure. Furthermore, it was observed that on GPR maps where two adjacent bars were investigated higher values of velocity were obtained than in radargrams where only single bars were scanned.
- Two or more adjacent bars caused deformation of the shape of the diffraction hyperbola as well as the change of its strength. The meaningful increase of the signal amplitude with the increasing number of adjacent bars was observed.

- The transverse rebar under the main reinforcement was represented in numerical radargram as a longitudinal reflection that cut-off diffraction hyperbolas at a certain depth. The detection of a transverse rebar over the main reinforcement was possible in both experimental and numerical radargrams. The reflection from the transverse bar appeared in the radargram as a line over a row of hyperbolas.

The novel approach presented in this paper is the use of 3-D FDTD numerical modelling in civil engineering applications. The three-dimensional model enabled obtaining radargrams along arbitrarily selected scan routes and analyzing spatial arrangements of rebars, which is unachievable in the case of two-dimensional modelling. Precise 3-D modelling of the complex reinforcement system in the considered bridge allowed to identify reflection and diffraction patterns accurately and enhance the interpretation of results of GPR surveys.

References

[1] J. Hoła, K. Schabowicz, State-of-the-art non-destructive methods for diagnostic testing of building structures – anticipated development trends, Arch. Civ. Mech. Eng. 10 (2010) 5–18. doi:10.1016/S1644-9665(12)60133-2.

[2] P. Gaydecki, L. Heathcote, A methodology to extract dimensional information from steel bars using a magnetic field imaging camera (mFIC), Meas. Sci. Technol. 21 (2010) 1–10. doi:10.1088/0957-0233/21/7/075501.

[3] G.F. Pla-Rucki, M.O. Eberhard, Imaging of Reinforced Concrete: State-of-the-Art Review, J. Infrastruct. Syst. 1 (1995) 134–141. doi:10.1061/(ASCE)1076-0342(1995)1:2(134).

[4] A.M. Alani, M. Aboutalebi, G. Kilic, Applications of ground penetrating radar (GPR) in bridge deck monitoring and assessment, J. Appl. Geophys. 97 (2013) 45–54. doi:10.1016/j.jappgeo.2013.04.009.

[5] D. Bęben, A. Mordak, W. Anigacz, Ground penetrating radar application to testing of reinforced concrete beams, Procedia Eng. 65 (2013) 242–247. doi:10.1016/j.proeng.2013.09.037.

[6] L. Xiang, H.-L. Zhou, Z. Shu, S.-H. Tan, G.-Q. Liang, J. Zhu, GPR evaluation of the Damaoshan highway tunnel: A case study, NDT E Int. 59 (2013) 68–76. doi:10.1016/j.ndteint.2013.05.004.

[7] J. Stryk, R. Matula, K. Pospisil, Possibilities of ground penetrating radar usage within acceptance tests of rigid pavements, J. Appl. Geophys. 97 (2013) 11–26. doi:10.1016/j.jappgeo.2013.06.013.

[8] J. Hugenschmidt, A. Kalogeropoulos, F. Soldovieri, G. Prisco, Processing strategies for high-resolution GPR concrete inspections, NDT E Int. 43 (2010) 334–342. doi:10.1016/j.ndteint.2010.02.002.

[9] R. González-Drigo, V. Pérez-Gracia, D. Di Capua, L.G. Pujades, GPR survey applied to Modernista buildings in Barcelona: The cultural heritage of the College of Industrial Engineering, J. Cult. Herit. 9 (2008) 196–202. doi:10.1016/j.culher.2007.10.006.

[10] D.J. Clem, T. Schumacher, J.P. Deshon, A consistent approach for processing and interpretation of data from concrete bridge members collected with a hand-held GPR device, Constr. Build. Mater. 86 (2015) 140–148. doi:10.1016/j.conbuildmat.2015.03.105.

[11] L. Zanzi, D. Arosio, Sensitivity and accuracy in rebar diameter measurements from dual-polarized GPR data, Constr. Build. Mater. 48 (2013) 1293–1301. doi:10.1016/j.conbuildmat.2013.05.009.

[12] V. Pérez-Gracia, R. González-Drigo, D. Di Capua, Horizontal resolution in a non-destructive shallow GPR survey: An experimental evaluation, NDT E Int. 41 (2008) 611–620. doi:10.1016/j.ndteint.2008.06.002.

[13] S. Yehia, N. Qaddoumi, S. Farrag, L. Hamzeh, Investigation of concrete mix variations and environmental conditions on defect detection ability using GPR, NDT E Int. 65 (2014) 35–46. doi:10.1016/j.ndteint.2014.03.006.

[14] M. Rucka, J. Lachowicz, M. Zielińska, GPR investigation of the strengthening system of a historic masonry tower, J. Appl. Geophys. 131 (2016) 94–102. doi:10.1016/j.jappgeo.2016.05.014.

[15] M. Solla, H. Lorenzo, F.I. Rial, A. Novo, Ground-penetrating radar for the structural evaluation of masonry bridges: Results and interpretational tools, Constr. Build. Mater. 29 (2012) 458–465. doi:10.1016/j.conbuildmat.2011.10.001.

[16] M. Solla, H. González-Jorge, M.X. Álvarez, P. Arias, Application of non-destructive geomatic techniques and FDTD modeling to metrical analysis of stone blocks in a masonry wall, Constr. Build. Mater. 36 (2012) 14–19. doi:10.1016/j.conbuildmat.2012.04.134.

[17] X. Xie, H. Qin, C. Yu, L. Liu, An automatic recognition algorithm for GPR images of RC structure voids, J. Appl. Geophys. 99 (2013) 125–134. doi:10.1016/j.jappgeo.2013.02.016.

[18] J. Li, Z. Zeng, L. Huang, F. Liu, GPR simulation based on complex frequency shifted recursive integration PML boundary of 3D high order FDTD, Comput. Geosci. 49 (2012) 121–130. doi:10.1016/j.cageo.2012.06.020.

[19] I. Giannakis, A. Giannopoulos, C. Warren, A Realistic FDTD Numerical Modeling Framework of Ground Penetrating Radar for Landmine Detection, IEEE J. Sel. Top. Appl. Earth Obs. Remote Sens. 9 (2015) 1–15. doi:10.1109/JSTARS.2015.2468597.

[20] N. Diamanti, A. Giannopoulos, M.C. Forde, Numerical modelling and experimental verification of GPR to investigate ring separation in brick masonry arch bridges, NDT E Int. 41 (2008) 354–363. doi:10.1016/j.ndteint.2008.01.006.

[21] J. Lachowicz, M. Rucka, Numerical modeling of GPR field in damage detection of a reinforced concrete footbridge, Diagnostyka. 17 (2016) 3–8.

[22] J. Lachowicz, M. Rucka, Experimental and Numerical Investigations for GPR Evaluation of Reinforced Concrete Footbridge, in: 16th Int. Conf. Gr. Penetrationg Radar, Hong Kong, 2016: pp. 1–6. doi:10.1109/ICGPR.2016.7572675.

[23] L. Mertens, R. Persico, L. Matera, S. Lambot, Automated Detection of Reflection Hyperbolas in Complex GPR Images with No A Priori Knowledge on the Medium, IEEE Trans. Geosci. Remote Sens. 54 (2016) 580–596. doi:10.1109/TGRS.2015.2462727.

[24] F. Sagnard, J.-P. Tarel, Template-matching based detection of hyperbolas in ground-penetrating radargrams for buried utilities, J. Geophys. Eng. 13 (2016) 491–504. doi:10.1088/1742-2132/13/4/491.

[25] D.W. Marquardt, An Algorithm for Least-Squares Estimation of Nonlinear Parameters, J. Soc. Ind. Appl. Math. 11 (1963) 431–441.

[26] A. Giannopoulos, Modelling ground penetrating radar by GprMax, Constr. Build. Mater. 19 (2005) 755–762. doi:10.1016/j.conbuildmat.2005.06.007.

[27] C. Warren, A. Giannopoulos, I. Giannakis, gprMax: Open source software to simulate electromagnetic wave propagation for Ground Penetrating Radar, Comput. Phys. Commun. 209 (2016) 163–170. doi:10.1016/j.cpc.2016.08.020.

[28] K.S. Yee, Numerical solution of initial boundary value problems involving Maxwell's equations in isotropic media, IEEE Trans. Antennas Propag. 14 (1966) 302–307. doi:10.1109/TAP.1966.1138693.

[29] J.F.C. Sham, W.W.L. Lai, Development of a new algorithm for accurate estimation of GPR's wave propagation velocity by common-offset survey method, NDT E Int. 83 (2016) 104–113. doi:10.1016/j.ndteint.2016.05.002.